Performance of Frequency Domain Multiuser-MIMO Turbo Equalization Without Cyclic Prefix

Takano, Yasuhiro

Su, Hsuan-Jung

Performance of Frequency Domain Multiuser-MIMO Turbo Equalization Without Cyclic Prefix

Yasuhiro Takano* and Hsuan-Jung Su†.
* Kobe University, 1-1 Rokkodai, Nada, Kobe, 657-8501, Japan.
† National Taiwan University, Taipei 10617, Taiwan.
e-mail: takano@eedept.kobe−u.ac.jp, hjs@ntu.edu.tw

Abstract—Multiuser (MU)-multiple-input multiple-output (MIMO) receivers often need to take iterative strategies to cancel multiuser-interference (MUI). Frequency domain turbo equalization is one of the most promising solutions to the MUI problem. It offers a reasonable trade-off between the receiver performance and the computational complexity by assuming cyclic prefix (CP)-transmission. Nevertheless, CP-transmission is not preferable for the battery life of user terminals. Therefore, this paper proposes a new frequency domain multiuser-detection (MUD) technique by extending the chained turbo equalization (CHATUE) to MU-MIMO systems. Simulation results verify that the proposed MU-MIMO CHATUE algorithm is a more reliable option to improve the spectral- and/or energy-efficiency by eliminating the necessity of CP-transmission than by shortening the training sequences or puncturing the coded data bits.

Index Terms—Spectral efficiency, multi-user interference (MUI), cyclic prefix (CP), overlap-and-add.

I. Introduction

Multiple-input multiple-output (MIMO) systems can improve the spectral efficiency by utilizing spatial multiplexing in the same time-frequency resource (e.g., [1]). However, received signals in Multiuser (MU)-MIMO systems suffer from multiuser interference (MUI) since the orthogonality of the channel parameters is not always guaranteed between users. Interference alignment (IA) approaches (e.g., [2]) are, therefore, extensively studied to improve the MUI. In Internet of Things (IoT) networks, etc., nevertheless, not all low-cost terminals are capable of ideally performing IA techniques. We may, hence, utilize iterative receiving strategy at base stations to combat the MUI problem. For example,

Authors' version as of 2018/Jul/30.

frequency domain turbo equalization techniques [3], [4] can perform multiuser detection (MUD) with reasonable computational complexity by assuming cyclic prefix (CP)-transmission. The CP is, nevertheless, an overhead for data transmission and is not preferable for the battery life of user terminals.

In oder to eliminate the necessity of CP-transmission, receivers may perform the overlap-and-add operation (e.g., [5]). It causes, nevertheless, the noise enhancement problem at the equalizer output. As a solution to the problem, CHATUE version 2 (CHATUE2) [6] algorithm has been studied in single user systems. Assuming no CP-transmission, the CHATUE2 performs computationally efficient frequency domain equalization without sacrificing receiver performance after sufficient turbo iterations. However, performance of the CHATUE2 receiver in MU-MIMO systems is not clarified yet. This paper proposes, therefore, a new MUD technique by extending the CHATUE2 to MU-MIMO systems. Simulation results verify MUD performance of the proposed technique when channel estimates are actually obtained in practical propagation scenarios.

This paper is organized as follows. Section II shows the system model assumed in this paper. Section III proposes the new MU-MIMO equalization technique. Section IV verifies the effectiveness of the proposed technique via computer simulation results. Section V shows concluding remarks.

II. System Model

An uplink MU-MIMO transmission system composed of U N_T-antenna users and an N_R-antenna base station is considered, where we refer to it as a $\{U, N_T\} \times N_R$ MU-MIMO system, hereafter. As depicted in Fig. 1, in the u-th transmitter, a length-N_{info} bit binary data information sequence $b_u(i)$ is channel-encoded into a coded frame $c_u(i_c)$ by a rate R_c convolutional code (CC) with generator polynomials $(g_1, \cdots, g_{1/R_c})$ and is interleaved by an interleaver (Π_u). The interleaved coded frame $c_u(\Pi_u(i_c))$ is serial-to-parallel (S/P)-converted

into N_T data segments for MIMO transmission using N_T transmission (TX) antennas. The data segments are modulated into quadrature phase shift keyed (QPSK) symbols[1] $x_{d,k'}^u(j_s;l)$ with variance σ_x^2 and the modulation multiplicity $M_b = 2$. For $k' = 1, \cdots, N_T$, the k'-th TX antenna transmits data symbols $\mathbf{x}_{d,k'}^u(l) = [x_{d,k'}^u(1;l), \cdots, x_{d,k'}^u(N_d;l)]^{\mathrm{T}}$ together with a length-N_t symbol training sequence (TS) $\mathbf{x}_{t,k'}^u(l)$ using single carrier signaling, where l denotes the slot timing index and the data symbol length N_d in a slot is defined as $N_d = N_{\text{info}}/(R_c N_T M_b)$.

The received signal $\mathbf{y}_n(l)$ at the n-th receive (Rx) antenna suffers from MUI and inter-symbol-interference (ISI) due respectively to multiuser access and fading frequency selectivity. Moreover, it suffers from complex additive white Gaussian noise (AWGN), too. The channel impulse response (CIR) length is at most W symbols. By assuming the guard interval (GI) length N_{G2} is grater than W, the received signals with N_R Rx antennas can be described in a matrix form as,

$$\mathcal{Y}(l) = \mathcal{H}(l)\mathcal{X}(l) + \mathcal{Z}, \tag{1}$$

where

$$
\begin{array}{rcll}
\mathcal{Y}(l) &=& [\mathbf{y}_1(l), \cdots, \mathbf{y}_{N_R}(l)]^{\mathrm{T}} &\in \mathbb{C}^{N_R \times \tilde{L}_{\mathrm{S}}}, \\
\mathcal{X}(l) &=& [\mathbf{X}_1^{\mathrm{T}}(l), \cdots, \mathbf{X}_{UN_T}^{\mathrm{T}}(l)]^{\mathrm{T}} &\in \mathbb{C}^{WUN_T \times \tilde{L}_{\mathrm{S}}}, \\
\mathcal{H}(l) &=& [\mathbf{H}_1(l), \cdots, \mathbf{H}_{UN_T}(l)] &\in \mathbb{C}^{N_R \times WUN_T}, \\
\mathcal{Z} &=& [\mathbf{z}_1, \cdots, \mathbf{z}_{N_R}]^{\mathrm{T}} &\in \mathbb{C}^{N_R \times \tilde{L}_{\mathrm{S}}}.
\end{array}
$$

We define the matrix size $\tilde{L}_{\mathrm{S}} = L_{\mathrm{S}} + W'$ with the slot length $L_{\mathrm{S}} = N_t + N_{\text{G1}} + N_{\text{CP}} + N_d + N_{\text{G2}}$ and the ISI length $W' = W - 1$. Let us denote index $k = k' + (u - 1)N_T$ corresponding to the k'-th TX stream of the u-th user. $\mathbf{X}_k(l)$ is given by

$$\mathtt{tplz}_W \left\{ [\mathbf{x}_{t,k'}^{u\,\mathrm{T}}(l), \mathbf{0}_{N_{\text{G1}}}^{\mathrm{T}}, \mathbf{x}_{\text{CP},k'}^{u\,\mathrm{T}}(l), \mathbf{x}_{d,k'}^{u\,\mathrm{T}}(l), \mathbf{0}_{N_{\text{G2}}+W'}^{\mathrm{T}}] \right\},$$

where $\mathbf{x}_{\text{CP},k'}^u$ is composed with the last N_{CP} entries of $\mathbf{x}_{d,k'}^u(l)$. The operation $\mathtt{tplz}_W\{\mathbf{r}\}$ constructs a $W \times N_r$ Toeplitz matrix whose first row vector is $\mathbf{r} \in \mathbb{C}^{1 \times N_r}$. The variance of the CIR sub-matrix is $\mathbb{E}[\|\mathbf{H}_k(l)\|^2] = \sigma_{\mathbf{H}}^2(\lceil k/N_T \rceil)$ with a constant $\sigma_{\mathbf{H}}^2(u)$ for the u-th user, where $\lceil \cdot \rceil$ indicates the ceiling function. Furthermore, the CIR satisfies a property that the spatial covariance matrix $\mathbb{E}[\mathbf{H}_k(l)\mathbf{H}_k^{\mathrm{H}}(l)]$ is of full-rank by assuming no unknown interferences from other cells [8]. The noise vector at the n-th Rx antenna $\mathbf{z}_n$ follows the Complex normal distribution $\mathcal{CN}(\mathbf{0}, \sigma_z^2 \mathbf{I}_{\tilde{L}_{\mathrm{S}}})$ and has the spatially uncorrelated property: $\mathbb{E}[\mathbf{z}_{n_1}^{\mathrm{H}} \mathbf{z}_{n_2}] = 0$ for $n_1 \neq n_2$.

As depicted in Fig. 1, the receiver performs channel estimation (EST) jointly over the Rx antennas while also obtaining the extrinsic log-likelihood ratio (LLR) $\lambda_{\mathrm{q},k}^e$ for the k-th TX stream by means of the CHATUE2 [6] (EQU) technique. The sequences $\lambda_{\mathrm{q},k}^e$ are parallel-to-serial (P/S)-converted to LLRs $\lambda_{\mathrm{EQU},u}^e$ corresponding to the interleaved coded frames $c_u(j_c)$ at the u-th

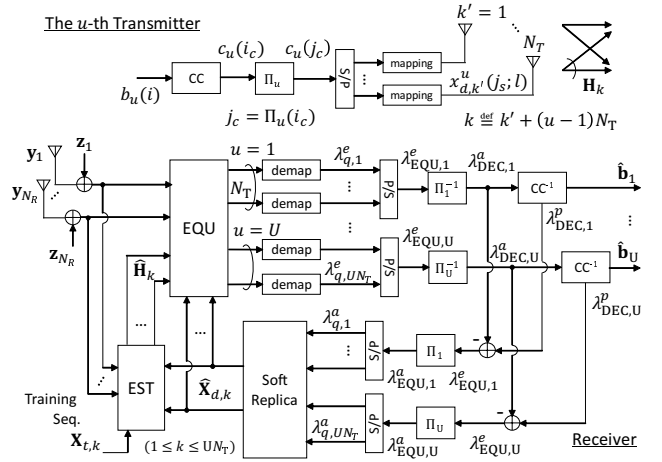[1]Extension to higher order modulation is straightforward [7].

Fig. 1. A $\{U, N_T\} \times N_R$ MU-MIMO system.

transmitter. An *a priori* LLR $\lambda_{\mathrm{DEC},u}^a$ for the channel decoder (CC^{-1}) is obtained by deinterleaving $\lambda_{\mathrm{EQU},u}^e$. The channel decoder performs decoding for $\lambda_{\mathrm{DEC},u}^a$ by using the Bahl, Cocke, Jelinek and Raviv (BCJR) algorithm [9], and outputs the *a posteriori* LLR $\lambda_{\mathrm{DEC},u}^p$. After several iterations, CC^{-1} outputs the estimates of the transmitted sequence $\hat{\mathbf{b}}$ by making a hard decision on $\lambda_{\mathrm{DEC},u}^p$.

EQU utilizes the soft replica[2] of the transmitted symbols $\hat{\mathbf{x}}_{d,k}$ which is generated from the equalizer's *a priori* LLR vector $\lambda_{\mathrm{EQU},\lceil k/N_T \rceil}^a$. Moreover, the LLR $\lambda_{\mathrm{EQU},u}^a$ is the interleaved version of the extrinsic LLR $\lambda_{\mathrm{DEC},u}^e$ given by $\lambda_{\mathrm{DEC},u}^p - \lambda_{\mathrm{DEC},u}^a$.

III. CHANNEL EQUALIZATION

A. Signal model

The signal model (1) is re-formulated to develop MU-MIMO channel equalization algorithms. The vectorized received data segment $\mathbf{y}_d(l) \in \mathbb{C}^{N_R \tilde{N}_d \times 1}$ can be described as

$$\mathbf{y}_d(l) = \mathbf{H}(l)\mathbf{s}(l) + \mathbf{z}_d \tag{2}$$

with the length $UN_T N_d$ signal vector $\mathbf{s}(l) = [\mathbf{x}_{d,1}^{\mathrm{T}}(l), \cdots, \mathbf{x}_{d,UN_T}^{\mathrm{T}}(l)]^{\mathrm{T}}$, where the noise vector $\mathbf{z}_d$ follows $\mathcal{CN}(\mathbf{0}_{N_R \tilde{N}_d}, \sigma_z^2 \mathbf{I}_{N_R \tilde{N}_d})$ with $\tilde{N}_d = N_d + W'$. The $N_R \tilde{N}_d \times UN_T N_d$ CIR matrix $\mathbf{H}(l)$ is defined as

$$\mathbf{H}(l) = \begin{bmatrix} \mathbf{H}_{\{1,1\}}(l) & \cdots & \mathbf{H}_{\{1,UN_T\}}(l) \\ \vdots & \ddots & \vdots \\ \mathbf{H}_{\{N_R,1\}}(l) & \cdots & \mathbf{H}_{\{N_R,UN_T\}}(l) \end{bmatrix}, \tag{3}$$

[2]In the case of QPSK, as shown in [7], the i-th entry in the soft replica vector $\hat{\mathbf{x}}_{d,k}(l)$ is generated as $\hat{x}_{d,k}(i;l) = \sqrt{\frac{\sigma_x^2}{2}}\{\tanh(\lambda_{\mathrm{q},k}^a(2i;l)/2) + \sqrt{-1}\tanh(\lambda_{\mathrm{q},k}^a(2i+1;l)/2)\}$, where $\lambda_{\mathrm{q},k}^a(i;l)$ denotes the i-th entry of the S/P-converted equalizer's *a priori* LLR $\lambda_{\mathrm{q},k}^a(l)$ for the k-th TX stream.

where the (i,j)-th submatrix $\mathtt{H}_{\{i,j\}}(l)$ denotes the $\tilde{N}_d \times N_d$ Toeplitz matrix whose first column vector is $[\mathbf{h}_{i,j}^{\mathrm{T}}(l)\ \mathbf{0}_{1 \times (\tilde{N}_d - W)}]^{\mathrm{T}}$ with $\mathbf{h}_{i,j}(l)$ being the length-W symbol CIR vector for the (i,j)-th Rx-TX link.

B. MIMO CHATUE2 Algorithm

1) Rx replica generation: An estimate vector corresponding to (2) can be obtained, as $\hat{\mathbf{y}}_d(l) = \hat{\mathtt{H}}(l)\hat{\mathbf{s}}(l)$, where we refer to $\hat{\mathbf{y}}_d(l)$ as *Rx replica* vector. The transmitted replica vector $\hat{\mathbf{s}}_k(l) = \hat{\mathbf{x}}_{d,k}(l)$ of the k-th data stream is computed by using $\lambda_{\mathrm{DEC},\lceil k/N_T \rceil}^{p}$ fed back from the decoder. The channel estimate matrix $\hat{\mathtt{H}}(l)$ can be obtained by using the $\ell 2$ minimum mean square error (MMSE) channel estimation technique [10].

2) Circulant property restoration: The received vector $\mathbf{y}_d(l)$ (2) does not have the circulant property since the channel parameter $\mathtt{H}(l)$ (3) is a Toeplitz matrix. The receiver needs to restore the circulant property in $\mathbf{y}_d(l)$ to utilize a low-complexity frequency domain equalization (FDE) technique. We may, hence, perform the overlap-and-add operation [5] for $\mathbf{y}_d(l)$. However, as discussed in [6], it suffers from the noise enhancement problem. As a solution to the problem, the CHATUE2 algorithm restores the circulant property in the received vector by combining $\mathbf{y}_d(l)$ and the Rx replica vector $\hat{\mathbf{y}}_d(l)$. Specifically, the *composite replica* [6] is defined by

$$\bar{\mathbf{r}}(l) = \tilde{\mathtt{J}}_{W'}(1-\beta)\mathbf{y}_d(l) + \tilde{\mathtt{G}}_{W'}(\beta)\hat{\mathbf{y}}_d(l) \quad (4)$$

with $\tilde{\mathtt{J}}_{W'}(1-\beta) = \mathbf{I}_{N_R} \otimes \mathtt{J}_{W'}(1-\beta)$ and $\tilde{\mathtt{G}}_{W'}(1-\beta) = \mathbf{I}_{N_R} \otimes \mathtt{G}_{W'}(1-\beta)$, where $N_d \times (N_d + W')$ matrices $\mathtt{J}_{W'}$ and $\mathtt{G}_{W'}$ are, respectively,

$$\mathtt{J}_{W'}(1-\beta) = \begin{pmatrix} \mathbf{O}_{(N_d - W') \times W'} & \mathbf{I}_{N_d} \\ (1-\beta)\mathbf{I}_{W'} & \end{pmatrix}, \quad (5)$$

$$\mathtt{G}_{W'}(\beta) = \begin{pmatrix} & \mathbf{O}_{(N_d - L) \times W'} \\ \mathbf{O}_{N_d} & \beta\mathbf{I}_{W'} \end{pmatrix}. \quad (6)$$

The optimal factor β can be derived from

$$\beta = \arg\min_{\beta} \mathbb{E}\left[\|\mathbf{c}_d(l) - \bar{\mathbf{y}}_d(l,\beta)\|^2\right], \quad (7)$$

where $\bar{\mathbf{y}}_d(l,\beta) = (1-\beta)\mathbf{y}_d(l) + \beta\hat{\mathbf{y}}_d(l)$ and $\mathbf{c}_d(l) = \mathtt{H}(l)\mathbf{s}(l)$. Since $\mathbf{c}_d(l) = \mathbf{y}_d(l) - \mathbf{z}_d$, the solution to (7) can be determined, as

$$\beta = \frac{\sigma_z^2 N_R \tilde{N}_d}{\|\mathbf{y}_d(l) - \hat{\mathbf{y}}_d(l)\|^2}, \quad (8)$$

in the MIMO signal model, according to the accuracy of the Rx replica $\hat{\mathbf{y}}_d(l)$.

3) Frequency domain MMSE equalization: We simultaneously cancel the MUI and the ISI by

$$\tilde{\mathbf{r}}(l) = \bar{\mathbf{r}}(l) - \tilde{\mathtt{J}}_{W'}(1)\hat{\mathbf{y}}_d(l). \quad (9)$$

The MIMO version of CHATUE2 algorithm performs the joint-over-antenna (JA) MIMO MMSE equalization

[3] for the residual vector $\tilde{\mathbf{r}}(l)$. The equalizer output of the MIMO CHATUE2 can be described, as

$$\mathbf{q}_k(l) = \left(\mathbf{I}_{N_d} + \mathbf{\Gamma}_k(l)\hat{\mathtt{S}}_k(l)\right)^{-1}$$
$$\cdot \left[\mathbf{\Gamma}_k(l)\hat{\mathbf{s}}_k(l) + \mathbf{F}_{N_R}^{\mathrm{H}}\mathbf{\Phi}_k^{\mathrm{H}}(l)\mathbf{\Omega}^{-1}(l)\mathbf{F}_{N_R}\tilde{\mathbf{r}}(l)\right] \quad (10)$$

for the k-th TX stream. The frequency domain CIR $\mathbf{\Phi}_k(l)$ is also described by using $\tilde{\mathtt{J}}_{W'}(\cdot)$-matrix, as

$$\mathbf{\Phi}_k(l) = \mathbf{F}_{N_R}\tilde{\mathtt{J}}_{W'}(1)\mathtt{H}_k(l)\mathbf{F}^{\mathrm{H}} \quad (11)$$

with $\mathbf{F}_N = \mathbf{I}_N \otimes \mathbf{F}$, where $\mathbf{F} \in \mathbb{C}^{N_d \times N_d}$ is the discrete Fourier transform (DFT) matrix whose $(r+1, c+1)$-th entry is $\exp(-2\pi rc\sqrt{-1}/N_d)/\sqrt{N_d}$ with integer indexes $0 \leq r, c \leq N_d - 1$. The CIR $\mathtt{H}_k(l)$ is the k-th column block matrix of (3). Note that (11) becomes an $N_R N_d \times N_d$ block diagonal matrix since $\tilde{\mathtt{J}}_{W'}(1)\mathtt{H}_k(l)$ is a circulant matrix.

The covariance matrix $\mathbf{\Omega}(l) \in \mathbb{C}^{N_R N_d \times N_R N_d}$ in (10) is computed, as

$$\mathbf{\Omega}(l) = \mathbf{F}_{N_R}\left\{\tilde{\mathtt{J}}_{W'}(1)\mathtt{H}(l)\mathbf{\Lambda}(l)\{\tilde{\mathtt{J}}_{W'}(1)\mathtt{H}(l)\}^{\mathrm{H}}\right.$$
$$\left. + \sigma_z^2\tilde{\mathtt{J}}_{W'}(1-\beta)\tilde{\mathtt{J}}_{W'}(1-\beta)^{\mathrm{H}}\right\}\mathbf{F}_{N_R}^{\mathrm{H}}$$
$$\approx \mathbf{\Phi}(l)\mathbf{\Delta}(l)\mathbf{\Phi}(l)^{\mathrm{H}} + \sigma_z^2\frac{N_d + (1-\beta)W'}{N_d}\mathbf{I}_{N_R N_d},$$
$$(12)$$

where $\mathbf{\Phi}(l) = [\mathbf{\Phi}_1(l), \cdots, \mathbf{\Phi}_{UN_T}(l)]$ and

$$\mathbf{\Lambda}(l) = \mathbb{E}\left[\{\mathbf{s}(l) - \hat{\mathbf{s}}(l)\}\{\mathbf{s}(l) - \hat{\mathbf{s}}(l)\}^{\mathrm{H}}\right],$$
$$\mathbf{\Delta}(l) = \mathrm{diag}\{[\delta_1(l)\mathbf{1}_{N_d}^{\mathrm{T}}, \cdots, \delta_{UN_T}(l)\mathbf{1}_{N_d}^{\mathrm{T}}]^{\mathrm{T}}\}$$

with $\delta_k(l) = \sigma_x^2 - \|\hat{\mathbf{s}}_k(l)\|^2/N_d$. In (10), moreover, $\tilde{N}_d \times \tilde{N}_d$ matrices $\mathbf{\Gamma}_k(l)$ and $\hat{\mathtt{S}}_k(l)$ are defined respectively, as

$$\mathbf{\Gamma}_k(l) = \frac{1}{N_d}\mathrm{tr}\left[\mathbf{\Phi}_k^{\mathrm{H}}(l)\mathbf{\Omega}^{-1}(l)\mathbf{\Phi}_k(l)\right]\mathbf{I}_{N_d} \quad (13)$$

$$\hat{\mathtt{S}}_k(l) = (\|\hat{\mathbf{s}}_k(l)\|^2/N_d)\mathbf{I}_{N_d}. \quad (14)$$

4) Extrinsic LLR transformation: The equalizer output $\mathbf{q}_k(l)$ is, finally, transformed into the extrinsic LLRs $\lambda_{\mathrm{EQU},u}^{e}(l)$ corresponding to the interleaved bit sequence $c_u(j_c)$ by using the P/S conversion and the Gaussian channel approximation. Specifically,

$$\lambda_{\mathrm{EQU},u}^{e}(l) = \mathrm{vec}\left\{\left[\ \lambda_{\mathrm{q},1+(u-1)N_T}^{e}(l), \cdots, \lambda_{\mathrm{q},uN_T}^{e}(l)\ \right]^{\mathrm{T}}\right\},$$

where, in the case the transmitted data sequence is modulated into QPSK symbols, the LLRs $\lambda_{\mathrm{q},k}^{e}(l)$ are given by [7], as

$$\lambda_{\mathrm{q},k}^{e}(l) = \frac{\sqrt{8}}{1 - \mu_{\mathrm{q},k}(l)}\mathrm{vec}\left\{\begin{bmatrix} \Re\{\mathbf{q}_k(l)\}^{\mathrm{T}} \\ \Im\{\mathbf{q}_k(l)\}^{\mathrm{T}} \end{bmatrix}\right\}. \quad (15)$$

$\Re\{\mathbf{v}\}$ and $\Im\{\mathbf{v}\}$ respectively denote the real and imaginary parts of the complex vector $\mathbf{v}$, and

$$\mu_{\mathrm{q},k}(l) = \frac{1}{N_d}\mathrm{tr}\left\{\mathbb{E}[\mathbf{q}_k(l)\mathbf{s}_k^{\mathrm{H}}(l)]\right\}$$
$$= \frac{\|\mathbf{s}_k(l)\|^2}{N_d^2}\mathrm{tr}\left\{(\mathbf{I}_{N_d} + \mathbf{\Gamma}_k(l)\hat{\mathtt{S}}_k(l))^{-1}\mathbf{\Gamma}_k(l)\right\}. \quad (16)$$

This is because the final output of CHATUE2 $q_k(l)$ can be approximated as an equivalent Gaussian channel output [11], [12] having input $s_k(l)$, as

$$q_k(l) = \mu_{q,k}(l)s_k(l) + z_{q,k}(l), \qquad (17)$$

where $z_{q,k}(l) \sim \mathcal{CN}(\mathbf{0}_{N_d}, \sigma_{q,k}^2(l)\mathbf{I}_{N_d})$ with

$$\sigma_{q,k}^2(l) = \mu_{qk}(l)(1 - \mu_{q,k}(l)). \qquad (18)$$

C. Computational complexity order

The proposed algorithm requires the complexity of order $\mathcal{O}(UN_T N_R N_d \log N_d)$. This is because, by using the subblock-wise diagonal structure, the calculation of $\mathbf{\Omega}^{-1}(l)$ can be reduced to N_d sub-problems of an $N_R \times N_R$ matrix inversion. The complexity needed for the equalizer output (10) is, hence, dominated by fast Fourier transform (FFT) operations.

It should be noted that the complexity order is equivalent to that of the conventional turbo equalization with CP-transmission (TEQ-CP) technique [3]. This is because $\hat{y}_d(l)$ can be obtained via subtracting the IBI components from the IFFT vector of the frequency domain response $[\mathbf{\Phi}_1(l), \cdots, \mathbf{\Phi}_{UN_T}(l)]\mathbf{F}_{UN_T}^{H}\hat{s}(l)$. Thus, the complexity needed for (8) is very minor.

IV. NUMERICAL EXAMPLES

A. Simulation Setups

1) Channel Models: The CIRs are generated with the spatial channel model (SCM) [13], [14]. This paper assumes $\{3, 2\} \times 6$ MIMO channels, where the antenna element spacing at the base station and the mobile station are, respectively, set at 4 and 0.5 wavelength. Spatial parameters such as the direction of arrival (DoA) are randomly chosen. Moreover, six path fading channel realizations based on the Pedestrian-B (PB) model [13] with a 3 km/h mobility (PB3) and the Vehicular-A (VA) model [13] with a 30 km/h mobility (VA30) are respectively assumed for the first user and the other two users. The path positions of the PB and VA models are respectively set at $\{1, 2.4, 6.6, 9.4, 17.1, 26.9\}$ and $\{1, 3.2, 6, 8.6, 13.1, 18.6\}$ symbol timings assuming that a TX bandwidth is 7 MHz with a carrier frequency of 2 GHz. However, the CIRs observed at the receiver can be distributed over more than 27 symbol duration due to the effect of the matched filtering. The maximum CIR length W is, hence, set at 31.

2) TX Formats: Table I shows details of the TX format parameters, where we assume $N_{\mathrm{G1}} = N_{\mathrm{G2}} = W$ to avoid the inter-block-interference (IBI) problem[3] in the received TS. All the three formats have $L_{\mathrm{S}} = 760$ symbol duration, and transmit $N_{\mathrm{info}} = 1024$ information bits after convolutional encoding with the generator polynomial $(g_1, g_2) = (7, 5)_8$. The TSs are generated

[3]The MU-MIMO CHATUE2 receiver using the chained turbo estimation (CHATES) [6] is expected to solve the IBI problem, although it remains as future work of this study.

TABLE I
TX FORMATS FOR A $\{3, 2\} \times 6$ MU-MIMO SYSTEM.

Format	N_{info}	N_t	N_{CP}	N_d	R_c	EQU
1	1024	186	0	512	1/2	CHATUE2
2	1024	186	32	480	8/15	TEQ-CP
3	1024	154	32	512	1/2	TEQ-CP

by using the first N_t bits of length 255 Gold sequences. The proposed MU-MIMO CHATUE2 algorithm assumes Format 1 without CP-transmission. Format 2 is used for the conventional TEQ-CP technique, where the CP-ratio is 0.0625. However, Format 2 is required to puncture the coded bits with puncturing ratio $15/16$ to assign the TX duration for the CP. Format 3 provides another option to allow CP-transmission in the limited TX duration by shrinking the TS section, where we suppose that a turbo receiver is expected to obtain CIR estimates accurately by jointly using the TS and the soft replica $\hat{x}_{d,k}$ of transmitted data after sufficient iterations.

B. Channel Estimation Performance

Fig. 2 shows normalized MSE (NMSE) performance of the $\ell2$ MMSE channel estimation technique in the MU-MIMO channel realizations, where NMSE $= \mathbb{E}[\|\hat{H}(l) - H(l)\|^2]/\mathbb{E}[\|H(l)\|^2]$ for channel estimates $\hat{H}(l)$. The normalized Cramér-Rao bound (CRB) is given by $\mathrm{NCRB}_{\bar{N}}(\sigma_z^2) = \sigma_z^2 \bar{r} UN_T N_R/\{\bar{N}\mathbb{E}[\|H(l)\|^2]\}$ for length $\bar{N}$ reference signals, where the parameters are set at $(U, N_T, N_R, \bar{r}) = (3, 2, 6, 6)$. As depicted in Fig. 2, the NMSE performance with Format 3 suffers from deterioration significantly in the first turbo iteration ($N_{\mathrm{turbo}} = 1$), since $N_t \geq WUN_T$ does not hold for Format 3. However, after performing 9 iterations ($N_{\mathrm{turbo}} = 9$), the $\ell2$ MMSE channel estimation using either three formats achieves the CRB asymptotically in a moderate to high signal-to-noise ratio (SNR) regime. This is because the $\ell2$ MMSE technique estimates the CIRs by jointly utilizing the TS and the soft replica $\hat{x}_k$ vectors. Hence, $\bar{N}_{td} \geq WUN_T$ holds after sufficient turbo iterations since the reference signal length converges to $\bar{N}_{td} = N_t + N_d - W'$.

C. EXIT Analysis

Fig. 3 depicts extrinsic information transfer (EXIT) charts to illustrate the convergence property of the proposed MU-MIMO CHATUE2 receiver, where 31-path Rayleigh fading channel realizations are assumed to observe general behavior of the proposed algorithm. The average SNR is set at 7 dB. We define the LLR's accuracy by the mutual information (MI) $\mathcal{I}_{\mathrm{EQU},u}^a = \mathcal{I}(\lambda_{\mathrm{EQU},u}^a; c_u)$ between the LLR $\lambda_{\mathrm{EQU},u}^a$ and the coded bits c_u at the transmitter by

$$\frac{1}{2}\sum_{\mathfrak{m}=\pm 1}\int_{-\infty}^{+\infty} \mathrm{P_r}(\lambda_{\mathrm{EQU},u}^a|\mathfrak{m})\log_2\frac{\mathrm{P_r}(\lambda_{\mathrm{EQU},u}^a|\mathfrak{m})}{\mathrm{P_r}(\lambda_{\mathrm{EQU},u}^a)} d\lambda_{\mathrm{EQU},u}^a,$$

where $\mathrm{P_r}(\lambda_{\mathrm{EQU},u}^a|\mathfrak{m})$ is the conditional probability
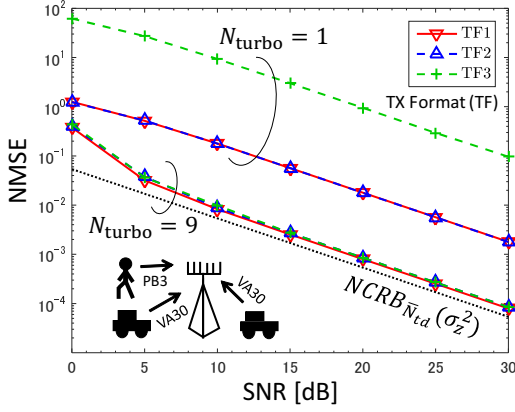
Fig. 2. NMSE performance of the $\ell 2$ MMSE channel estimation technique in the $\{3, 2\} \times 6$ MU-MIMO receiver.

Fig. 3. EXIT charts in 31-path Rayleigh fading channels. SNR is set at 7 dB.

density of $\lambda_{\mathrm{EQU},u}^a$ given $\mathfrak{m} = 1 - 2c_u$ [12]. For the sake of simplicity, this subsection assumes that all users take the same MI $\mathcal{I}_{\mathrm{EQU},u}^a$.

We first focus on investigating equalizer's EXIT convergence performance by assuming $\mathcal{I}_{\mathrm{EST},u}^a = 1$, so that channel estimates are obtained with ideal precision using long reference signals. As shown in Fig. 3, when $\mathcal{I}_{\mathrm{EST},u}^a = 1$, the EXIT curve obtained with the TEQ-CP approximately achieves $\mathcal{I}_{\mathrm{EST},u}^e = 1$ as $\mathcal{I}_{\mathrm{EST},u}^a$ tends to 1. The EXIT curve using the CHATUE2 also attains $\mathcal{I}_{\mathrm{EST},u}^e \approx 1$ as $\mathcal{I}_{\mathrm{EST},u}^a \rightarrow 1$ by improving β in the problem (7). However, at $\mathcal{I}_{\mathrm{EST},u}^e = 0$, it suffers from degradation although very slightly. This is because the noise enhancement at the CHATUE2 output is described by the trace norm of the second term in (12), and it becomes very minor when $W' \ll N_d$ and vanishes as $\beta \rightarrow 1$.

The EXIT convergence performance taking account of channel estimation errors is, then, discussed by letting $\mathcal{I}_{\mathrm{EST},u}^a = \mathcal{I}_{\mathrm{EQU},u}^a$ using imperfect reference signals. It is found from Fig. 3 that the equalizer's EXIT curves are deteriorated significantly due to the effect of channel estimation errors caused by the pilot contamination problems [15]. Recall that, because of CP-transmission in the limited frame length, we have to use the channel code with $R_c = 8/15$ or to shorten the TS length. As shown in Fig. 3, the EXIT curve using the TEQ-CP with Format 2 intersects with that of the decoder at the $(0.05, 0.3)$ MI point. The TEQ-CP with Format 3 uses the half-rate code. Hence, the EXIT curve can reach $\mathcal{I}_{\mathrm{EQU},u}^e \approx 1$. However, the equalizer's curve intersects with that of the decoder at the $(0, 0.1)$ MI point. The EXIT curve using the CHATUE2 with Format 1 does not tangent to the corresponding half-rate decoder's curve. An EXIT trajectory of the CHATUE2 receiver is, hence, expected to achieve the $(1, 1)$ MI point after sufficient turbo iterations, even when the channel estimation is actually performed.
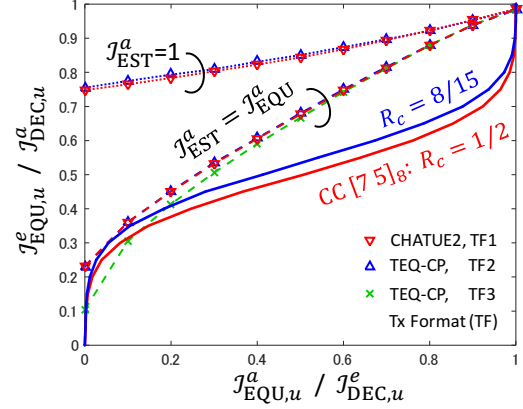
D. BER Performance

The average SNR is defined in association with the average energy per bit to noise density ratio $(\mathrm{E_b/N_0})$ as

$$\mathrm{SNR} = \sigma_x^2 \left(\mathbb{E}[\sigma_{\mathbf{H}}^2(u)]/N_R \right) \eta \cdot \mathrm{E_b/N_0} \quad (19)$$

with $\sigma_x^2 = 1$, where the spectral efficiency η of the TX format structure is given by $\eta = U N_{\mathrm{info}}/L_S$. The three TX formats have, thereby, the same spectral efficiency $\eta = 4$.

Fig. 4 shows bit error rate (BER) performance in the $\{3, 2\} \times 6$ MIMO system. In the case the channel parameter matrix $\mathbf{H}$ is known, the TEQ-CP with Format 3 obtains BER $= 10^{-5}$ at $\mathrm{E_b/N_0} = 10$ dB. The CHATUE2 with Format 1 achieves almost the same BER performance as that of TEQ-CP with Format 3. As shown in Fig. 5, it obtains BER $= 10^{-5}$ in five iterations. This is because, as discussed in Section IV-C, the noise enhancement of the MU-MIMO CHATUE2 algorithm is very minor when $W' \ll N_d$.

When channel estimation is performed, however, the TEQ-CP with Format 3 suffers from BER deterioration more than 1 dB against that of known $\mathbf{H}$ even after performing 9 iterations. This is because, as depicted in Fig. 3, the equalizer's EXIT curve using Format 3 of the short TS length intersects with the decoder's curve in a low MI $\mathcal{I}_{\mathrm{EQU},u}^a$ regime. However, after performing 9 iterations, the CHATUE2 receiver achieves gain more than 0.5 dB at BER $= 10^{-5}$ over the TEQ-CP receivers with Formats 2 and 3. This is because the CHATUE2 using Format 1 with the TS length $N_t = WUN_T$ does not suffer from the serious impact of channel estimation errors, and moreover, it can improve the error correction capability by using TX duration assigned for the CP. Therefore, even when channel estimation is actually performed, the MU-MIMO CHATUE2 algorithm enables us to improve the spectral- and/or energy-efficiency.
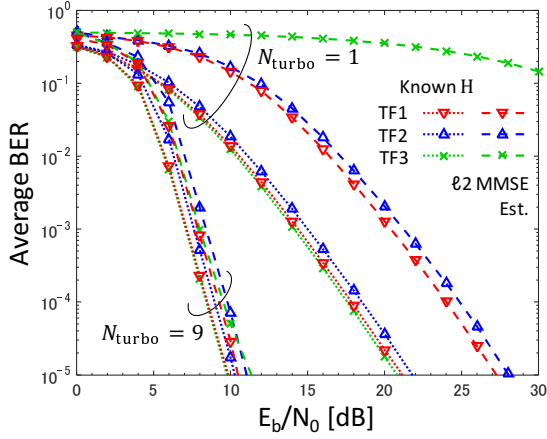
Fig. 4. Average BER performance in the $\{3, 2\} \times 6$ MIMO channels. The TX format (TF) 1 is used for the CHATUE2, whereas TFs 2 and 3 are assumed for the TEQ-CP receiver. All receivers perform the $\ell2$ MMSE channel estimation technique.
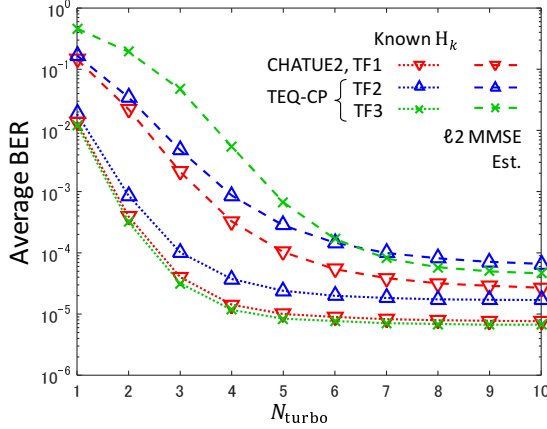

Fig. 5. BER convergence performance over turbo iterations. E_b/N_0 is set at 10 dB.

V. CONCLUSIONS

This paper has proposed a new frequency domain MU-MIMO equalization technique without CP-transmission by extending the CHATUE2 to the MUD scheme. The proposed algorithm restores the circulant property in the received signals by utilizing the composite replica composed of the received signals and the soft replica of TX symbols, without sacrificing the receiver performance. Hence, it allows us to have a long TS length and/or to improve the error correction capability by utilizing the TX duration assigned for CP.

The overhead of CP-transmission can, of course, be absorbed by puncturing coded bits or by shrinking the TS length under the assumption that a turbo channel estimation technique eventually obtains accurate CIR estimates after sufficient iterations. Simulation results show that, however, the CHATUE2 receiver achieves a BER gain of more than 0.5 dB over the other two

options when CIRs are actually estimated in $\{3, 2\} \times 6$ MU-MIMO transmission scenarios. This is because, as investigated in the EXIT analysis, the noise enhancement of the CHATUE2 is very minor compared to the coding loss due to the puncturing. Moreover, it has been verified that the MU-MIMO system should not shorten the TS length unnecessarily not to deteriorate the pilot contamination problem further. Therefore, the MU-MIMO CHATUE2 algorithm enables us to improve the spectral- and/or energy-efficiency even when channel estimation is actually performed.

REFERENCES

[1] N. I. Miridakis and D. D. Vergados, "A survey on the successive interference cancellation performance for single-antenna and multiple-antenna OFDM systems," *IEEE Commun. Surveys Tuts.*, vol. 15, no. 1, pp. 312–335, First 2013.

[2] N. Zhao, F. R. Yu, M. Jin, Q. Yan, and V. C. M. Leung, "Interference alignment and its applications: A survey, research issues, and challenges," *IEEE Commun. Surveys Tuts.*, vol. 18, no. 3, pp. 1779–1803, thirdquarter 2016.

[3] J. Karjalainen, N. Veselinovic, K. Kansanen, and T. Matsumoto, "Iterative frequency domain joint-over-antenna detection in multiuser MIMO," *IEEE Trans. Wireless Commun.*, vol. 6, no. 10, pp. 3620–3631, October 2007.

[4] R. Visoz, A. O. Berthet, and S. Chtourou, "Frequency-domain block turbo-equalization for single-carrier transmission over MIMO broadband wireless channel," *IEEE Trans. Commun.*, vol. 54, no. 12, pp. 2144–2149, Dec 2006.

[5] D. Wang, C. Wei, Z. Pan, X. You, C. H. Kyu, and J. B. Jang, "Low-complexity turbo equalization for single-carrier systems without cyclic prefix," in *Communication Systems, 2008. ICCS 2008. 11th IEEE Singapore International Conference on*, Nov. 2008, pp. 1091 –1095.

[6] Y. Takano, K. Anwar, and T. Matsumoto, "Spectrally efficient frame-format-aided turbo equalization with channel estimation," *IEEE Trans. Veh. Technol.*, vol. 62, no. 4, pp. 1635–1645, May 2013.

[7] M. Tüchler, A. Singer, and R. Koetter, "Minimum mean squared error equalization using a priori information," *IEEE Trans. Signal Process.*, vol. 50, no. 3, pp. 673–683, Mar 2002.

[8] M. Nicoli, O. Simeone, and U. Spagnolini, "Multislot estimation of fast-varying space-time communication channels," *IEEE Trans. Signal Process.*, vol. 51, no. 5, pp. 1184 – 1195, may 2003.

[9] L. Bahl, J. Cocke, F. Jelinek, and J. Raviv, "Optimal decoding of linear codes for minimizing symbol error rate (Corresp.)," *IEEE Trans. Inf. Theory*, vol. 20, no. 2, pp. 284 – 287, Mar. 1974.

[10] Y. Takano, M. Juntti, and T. Matsumoto, "$\ell1$ LS and $\ell2$ MMSE-based hybrid channel estimation for intermittent wireless connections," *IEEE Trans. Wireless Commun.*, vol. 15, no. 1, pp. 314–328, Jan 2016.

[11] X. Wang and H. Poor, "Iterative (turbo) soft interference cancellation and decoding for coded CDMA," *IEEE Trans. Commun.*, vol. 47, no. 7, pp. 1046 –1061, Jul. 1999.

[12] S. ten Brink, "Convergence behavior of iteratively decoded parallel concatenated codes," *IEEE Trans. Commun.*, vol. 49, no. 10, pp. 1727 –1737, Oct. 2001.

[13] European Telecommunications Standards Institute (ETSI), "Spatial channel model for MIMO simulations (3GPP TR 25.996)," Jan. 2017.

[14] J. Salo, G. Del Galdo, J. Salmi, P. Kyosti, M. Milojevic, D. Laselva, and C. Schneider, "MATLAB implementation of the 3GPP spatial channel model (3GPP TR 25.996)," On-line, Jan. 2005, http://www.ist-winner.org/3gpp_scm.html.

[15] Y. Takano, M. Juntti, and T. Matsumoto, "Performance of an $\ell1$ regularized subspace-based MIMO channel estimation with random sequences," *IEEE Wireless Commun. Lett.*, vol. 5, no. 1, pp. 112–115, Feb 2016.